Active Magnetic Regenerative Cooling with Smaller Magnets

Lucas Griffith[1] (corresponding author), Agata Czernuszewicz[1], Julie Slaughter[1], Vitalij Pecharsky[1,2]

[1] Ames Laboratory, U.S. Department of Energy, Iowa State University, Ames IA 50011-2416, USA

[2] Department of Materials Science and Engineering, Iowa State University, Ames IA 50011-2300, USA

Highlights

- Improved alignment of magnetic field and fluid flow raises efficiency
- Experiments prove the insensitivity of device performance to magnetic field profile
- Overall, results show efficiency can be conserved while halving magnet volume, cost

Abstract

Magnetocaloric heat pumping near room temperature, a.k.a. magnetic cooling, relies on the active regenerator cycle to achieve functional temperature spans and realize economic and societal benefits promised by this emerging solid-state cooling technology. The cycle itself depends upon synchronizing oscillating flow of a heat transfer fluid through a solid porous active material matrix, or the refrigerant, with periods when the refrigerant is in the highest available (field-on) and in nearly zero (field-off) magnetic fields to accomplish heat transfer. With this in mind, we analyze varying flow and magnetic field wave forms and the timing between when the fluid is pumped and when the magnetic field is turned on and off. We demonstrate that the volume and the cost of permanent magnet generating the field changes can be cut nearly in half with little to no effect on the device temperature span and cooling power normalized by the refrigerant mass.

Graphical Abstract

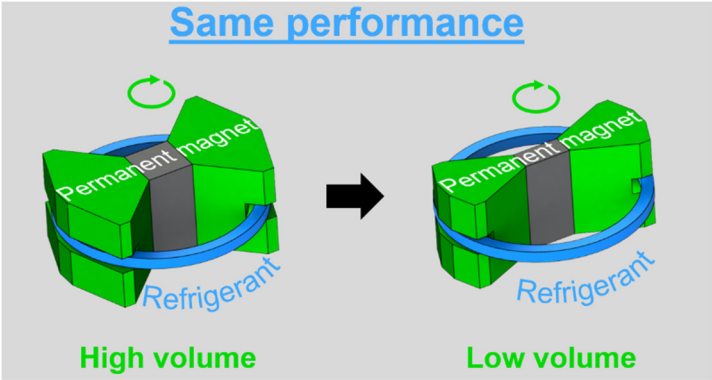

Keywords: active magnetic regeneration, magnetocaloric materials, magnetocaloric systems, second-law efficiency, permanent-magnet arrays

Nomenclature

t	Time (s)
b	Magnetic field profile balance parameter
P	Power (W)
ΔP	Pressure drop (Pa)
T	Temperature (K)
V_a	Angular velocity (revolutions s^{-1})
$\dot{V}$	Volumetric flow rate (m^3 s^{-1})

Subscripts and abbreviations

c	Cold (temperature) or cycle (time)
d	Delay (time) or device (power)
Ex	Exergetic
h	High (magnetic field) or hot (temperature)
p	Pump
r	Rest
COP	Coefficient of performance

Greek symbols

η	Second-law efficiency
ϕ	Pump fraction

1. Introduction

With over a century of research and development, vapor compression cooling technology [1], which almost exclusively supplies our cooling and refrigeration needs, is nearing its efficiency limits [2]. At the same time, global demand for cooling is growing rapidly with the number of air conditioning units deployed projected to triple in the next 30 years [3], owing largely to economic growth in densely inhabited areas. For this growth to be sustainable, considerable improvements in cooling efficiency must come to pass, in all likelihood by fundamentally changing the underlying technology similar to the recent shift in lighting from (gaseous) fluorescent tubes and bulbs to (solid) light-emitting diodes. Sensible alternatives to vapor compression must provide the necessary efficiency and scale while also offering safe operation and environmentally benign components.

Of the choices that could possibly satisfy these requirements while providing equally robust and versatile cooling as vapor compression, caloric heat pumping stands out as one of the most promising [4]. The Active Magnetic Regenerator (AMR) approach is the most mature of several caloric methodologies, with select heat pumps demonstrating coefficients of performance (COPs, defined as the ratio of cooling power to the power required to run the system) as high as 3.6 at 15.5 K temperature span [5]. One of the key barriers to adoption, however, is the high volume and cost of permanent magnet arrays required to create magnetic fields strong enough to drive the limited pool of currently available refrigerants [6].

To achieve heat pumping, magnetocaloric devices employ a Brayton-like thermodynamic cycle, known as the AMR cycle [7]. Assuming a direct magnetocaloric effect [8], the AMR cycle consists of four steps applied cyclically: 1) a magnetic field is applied to the active material, reducing its entropy through alignment of atomic magnetic moments (often accompanied by crystallographic changes) and increasing its temperature; 2) heat exchange fluid is forced from the cold end of the device toward the hot end, where it expels the heat absorbed from the active material; 3) the magnetic field around the material is removed, reversibly disordering the magnetic moments, increasing the refrigerant's entropy and decreasing its temperature; 4) chilled by the active material below the cold-side temperature, the heat exchange fluid is then forced from the hot end to a cold side heat exchanger where it can absorb heat.

Given the high cost of magnets, it is important to maximally harness the magnetic energy stored in the permanent magnet arrays for cooling. One important avenue toward this end is exploring the relationship between the magnetic field profile and the heat exchange fluid flow profile on regenerator performance. Hence, in this work, we fully define

and systematically control the magnetic field and fluid flow profiles, then measure the resulting temperature span delivered by the regenerator for different applied cooling loads. We also use finite-difference heat transfer modeling to support the experimental results and enable exploration of magnetic field profiles we could not achieve experimentally. Overall, the results show that the volume of permanent magnet required to drive a given volume of refrigerant can be halved with little or no penalty to device performance.

2. AMR Cycle Timing

Figure 1 shows schematic magnetic field and fluid flow profiles (waveforms) together with a few important timing parameters. They are the time spent at high field, t_h; the time spend at low field, t_l; the delay time, t_d; the pumping time (also known as the blow time), t_p; and the rest time, t_r. For convenience, the t_l and t_h are defined as the time during which the magnetic field experienced by the regenerator is within 3.5% of the full change in magnetic field of its minimum and maximum values respectively. For the CaloriSMART [9] employed here, this is when the magnetic field is within 0.05 T of the 0 and 1.45 T extrema. We define t_d as the delay between the beginning of t_l and the beginning of t_p with negative values indicating the flow begins before the magnetic field is within 3.5% of its minimum value. Commonly, t_p and t_r are combined into a single parameter, ϕ_p, called the pump fraction (or blow fraction) [10–12],

$$\phi_\mathrm{p} = \frac{t_\mathrm{p}}{t_\mathrm{p} + t_\mathrm{r}}. \qquad (1)$$

Similarly, we define a balance parameter, b, for the magnetic field profile such that $b = 1$ (fully balanced) when $t_\mathrm{h} = t_\mathrm{l}$, increasing from 0 to 2 as t_h increases relative to t_l,

$$b = 1 - \frac{t_\mathrm{l} - t_\mathrm{h}}{t_\mathrm{l} + t_\mathrm{h}}. \qquad (2)$$

Nearly every reported magnetocaloric heat pump uses a different magnetic field source, and therefore each has its own, unique magnetic field

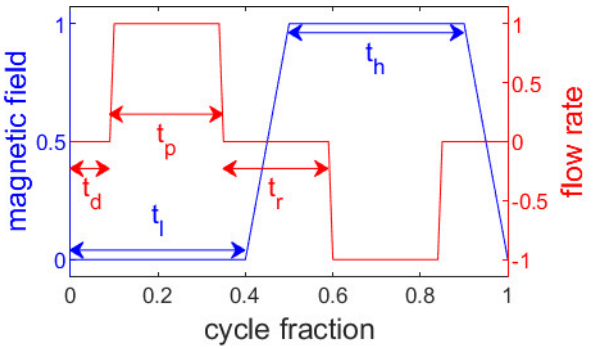

Figure 1 – Schematic of magnetic field and fluid flow profiles normalized by the corresponding maximum values showing the time at high field (t_h), the time at low field (t_l), the pumping time (t_p), the rest time (t_r) and the delay time (t_d).

waveform, and therefore, b. Yet, different devices employing elemental gadolinium as the refrigerant achieve similar maximum values of the exergetic power quotient [9], which normalizes temperature span and cooling power by the power available from the magnetic field, despite their conspicuously different magnetic field profiles.

Considering the time dependence of heat transfer in the active magnetic regenerator can help shed some light on this apparent insensitivity to the magnetic field profile. The temperature changes in gadolinium due to varying magnetic field are practically instantaneous, with little change in the overall magnitude at frequencies up to 22 Hz [13], well above typical device operating frequencies of 1 to 2 Hz. Engelbrecht *et al*. analyzed the operating frequency dependence of the resistances to heat transfer inside spherical particles and at their surfaces [14]. They analyzed both sinusoidal and step waveforms and found that sinusoidal waveforms have higher heat transfer resistance at any given frequency due to reduced time-averaged temperature difference between the refrigerant and the heat transfer fluid during pumping times in steps 2 and 4 of the AMR cycle.

Using the method of Ref. [14], we estimate the overall resistance to heat transfer reduces the heat transfer efficiency by only about three percent for a typical sphere diameter of 0.5 mm, with a sinusoidal waveform at 2 Hz operating frequency.

By using the heat transfer coefficient fitted to the oscillating fluid flow present in regenerators [15], which is significantly lower than that for developed flow [16], this provides a high-side estimate of the drop in efficiency. Therefore, at typical operating frequencies, neither the dynamics of the magnetocaloric effect itself nor heat transfer limitations from temperature gradients within the active material ought to present noticeable restrictions on device performance. For any particular magnetic field profile, however, the fluid flow profile must be adjusted to match.

The current understanding of the effect of the magnetic field and fluid flow profiles on cooling performance comes from a handful of modeling and experimental reports. Bjørk and Engelbrecht [17] as well as Fortkamp *et al.* [18] model the effect of the magnetic field ramp rate and t_h on maximum cooling power and temperature span. While the former study focuses on $b \leq 1$ and the latter focuses on $b \geq 1$, they both conclude that a balanced magnetic field profile with a rapid transition between high and low magnetic fields gives the best performance. For varying magnetic field profiles, both modeling studies align the center of t_p with the centers of both t_l and t_h, henceforth referred to as centered field and flow profiles. Bjørk and Engelbrecht further model the effect of t_d on maximum cooling power and temperature span for a fixed magnetic field profile [17]. Their results point toward centered profile alignment. Large t_d (or a shift of the fluid flow profile to the right in Figure 1) can result in fluid flow while the magnetic field starts reversing direction, thus disrupting the temperature gradient across the regenerator and reducing the estimated maximum cooling power. With t_h and t_l of only 25% cycle fraction, displacing the fluid flow by 10% reduces the maximum cooling power by 20 to 40% [17]. The effect on the cooling power for a range of t_d between the aligning the centers of t_p and t_l and aligning their ends is, however, minimal.

Benedict *et al.* vary frequency concurrently with t_d, making the results of t_d alone difficult to interpret [19]. Teyber *et al.* look at the effect of pump fraction on the performance of their device [10]. At a fixed operating frequency of 0.8 Hz, they adjust the pump fraction by diverting flow through an external circuit to concentrate the flow during times when the magnetic field is near its extrema. The main result is that exergetic cooling power can be increased by diverting flow to achieve smaller values of the pump fraction, however only at the cost of device efficiency. Fortkamp *et al.* [11] realized more direct control over the pump fraction by adjusting the cam ring timings for the poppet valves on their device. Similarly, they show that for a given cooling power, a higher temperature span can be achieved with a smaller pump fraction, but again at the cost of reduced device efficiency. Both studies adjusted the delay time, t_d, to center the field and flow profiles as suggested previously, comparable to the synchronization of the two profiles illustrated in Figure 1.

Here we provide a consistent, comprehensive study of the effects of controlling the magnetic field and fluid flow profiles by using the same device, the CaloriSMART [9], to individually vary each parameter. The fully digital control of the magnetic field and fluid flow profiles allows facile, robust control over both. The unique design of CaloriSMART allows modulation of the angular frequency of the permanent magnet assembly, providing the first in-depth look at the effect of varying the magnetic field profile on regenerator performance. The times the regenerator spends at high field and low field range from a well-balanced profile, with $t_\mathrm{h} = 0.25$ s and $t_\mathrm{l} = 0.27$ s ($b = 0.96$), to an imbalanced profile, with $t_\mathrm{h} = 0.49$ s and $t_\mathrm{l} = 0.14$ s ($b = 1.56$), at a constant operating frequency of 1 Hz. The advantages of balancing t_h and t_l are compared against the possibility for more economical magnet design. Pump fractions of 0.3 to 0.8 are explored with delay times on either side of those which center the magnetic field and fluid flow profiles. We show that

device performance can be improved by moving away from centering the magnetic field and fluid flow profiles. This adjustment eliminates the cooling power and temperature span limitations at high pump fractions described earlier [10,11].

3. Methods

3.1 Experimental

Data were collected using the CaloriSMART with a single active magnetic regenerator containing 24.7 g of 200 µm diameter spherical Gd particles as active material in an approximately 5 mL packed bed with a porosity of 0.36 as described previously [9]. The rotating permanent magnet assembly used to apply the magnetic field generates a maximum field of 1.45 T. Fluid flow is driven by a dual opposed syringe pump actuated by a linear motor. Motion of the rotating magnet assembly and the pump is coordinated by a rotary position encoder mounted to the magnet. A hot side temperature of 300.7 ± 0.5 K is maintained in all the experiments with a water bath connected to a tube-in-tube heat exchanger on the hot side. On the cold side, a cartridge heater provides simulated cooling loads up to 20 W. Flow on the hot and cold sides is unidirectional, with about 0.32 mL of space on either side of the regenerator to distribute the flow uniformly. Temperature is monitored at the inlets and outlets on the hot and cold side of the regenerator by four T-type thermocouples. The temperature span is defined as the difference between the hot side inlet, T_{h}, and the cold side inlet, T_{c}, since this is the temperature span over which heat can be pumped by the device. Pressure was measured on both sides of the AMR by absolute pressure transducers. Further details about the equipment are available elsewhere [9].

The values of t_{h} and t_{l} for the permanent magnet assembly are based on the magnetic field measured at the center of the regenerator. Figure 2 shows the measured magnetic field profiles and the input flow profiles with their centers aligned on the magnetic field profile. The t_{h} is 0.34 and the t_{l}

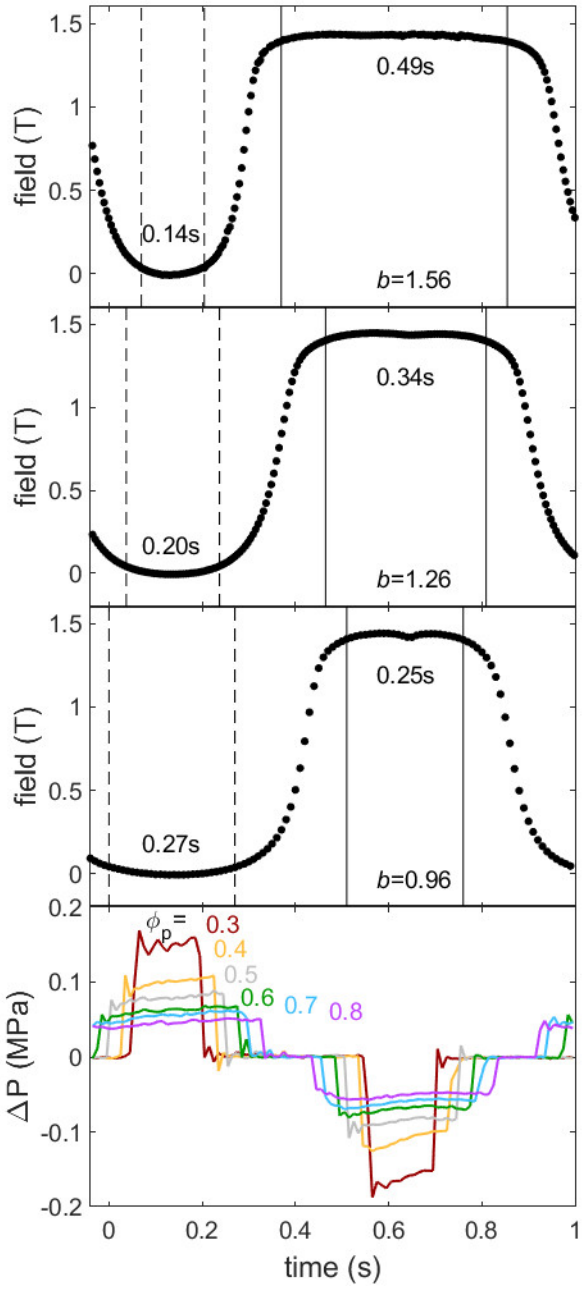

Figure 2 – Magnetic field vs. time measured at the center of the AMR bed for 1 Hz operation with vertical dashed lines indicating the time spent within 0.05 T of the field minimum and vertical solid lines showing the time spent within 0.05 T of the field maximum (top). The measured pressure drop across the regenerator vs. time for different pump fractions, ϕ_{p}, centered on the magnet profile (bottom).

is 0.2 when spun at a constant angular velocity, V_a, corresponding to an operating frequency of 1 Hz; b = 1.26 at any V_a = constant. These values can be adjusted by changing the V_a of the magnet as it spins. Applying constant acceleration and

deceleration between a higher V_a when the AMR is in the high field region and a lower V_a when the AMR is in the low field region makes the two values nearly equal (b = 0.96) as shown in Figure 2. Similarly, the two are further unbalanced by setting a higher V_a when the AMR is in the low field region and a lower V_a when the AMR is in the high field region, which results in b = 1.56.

These two modulated angular velocity profiles are executed by uploading a position vs. time table to the magnet motor controller. The table is executed every time the magnet passes its index pulse (once per revolution), maintaining synchronization between the actual position of the magnet and the velocity profile. The compliance and backlash of the gearbox between the magnet motor and the magnet assembly prevented any further changes to the magnetic field profile.

Similar to the magnet, the position of the pump is controlled via a lookup table. The position of the pump is driven by the position of the magnet rather than the time. Though the magnet can be accelerating or decelerating during a flow period, smooth motion of the pump is achieved by using the magnet motor profile to correct the values passed to the pump motor.

3.2 Numerical Modeling

Numerical methods used for heat transfer modeling were developed elsewhere, and the reader is referred to references [15, 20] for detailed descriptions. The model uses a 1-D finite difference method implemented in MATLAB to solve the convective heat equation for water flowing through a porous matrix of gadolinium. It models the magnetocaloric effect by approximating the entropy of gadolinium as a function of temperature and applied magnetic field. Nusselt number correlations for packed spherical beds [16], modified to account for temperature gradients in the spheres [15], estimate the heat transfer coefficient. Generally, conditions for modeling were set to closely match experimental conditions as shown in the supplemental information in Table S1.

4. Results

4.1 Magnetic Field Profile

Performance for balance parameters of 1.56, 1.26 and 0.96 is explored in Figure 3 in terms of the cooling power vs. temperature span at a pump fraction of 0.6, with a t_{d} that aligns the centers of the magnetic field and fluid flow profiles. The flow volumes of 2, 3, and 4 mL correspond to utilizations of 0.95, 1.43, and 1.91, respectively [9]. The lines for a given flow volume in Figure 3 are drawn by fitting (minimum r^2 of 0.987) measured temperature spans at four different applied cooling loads ranging from zero to the maximum, the latter is defined as the load that drives the temperature span near zero. The cooling performance achieved with the three different balance parameters is only slightly different. Results for $b = 1.56$ at a frequency of 1.5 Hz were not attainable with our equipment. To visualize the difference in performance, the maximum exergetic cooling power, P_{Ex}, which combines the temperature span between the hot-side temperature, T_{h}, and the cold side temperature, T_{c}, and the cooling power pumped from the cold side to the hot side, P,

$$P_{\mathrm{Ex}} = P\left(\frac{T_{\mathrm{h}}}{T_{\mathrm{c}}} - 1\right) \tag{3}$$

is compared for the three magnetic field profiles in Figure 4. Error in the exergetic cooling power is estimated based on a 90% confidence interval for linear fits to the temperature span vs. cooling power data at each flow volume. The maximum error estimated in this way is 2×10^{-5} W, which means that the difference in performance between the magnetic profiles is statistically significant compared to the variability in performance of this regenerator. That being said, the exergetic cooling

power at b = 1.56 is only about 10% less than that for b = 0.96.

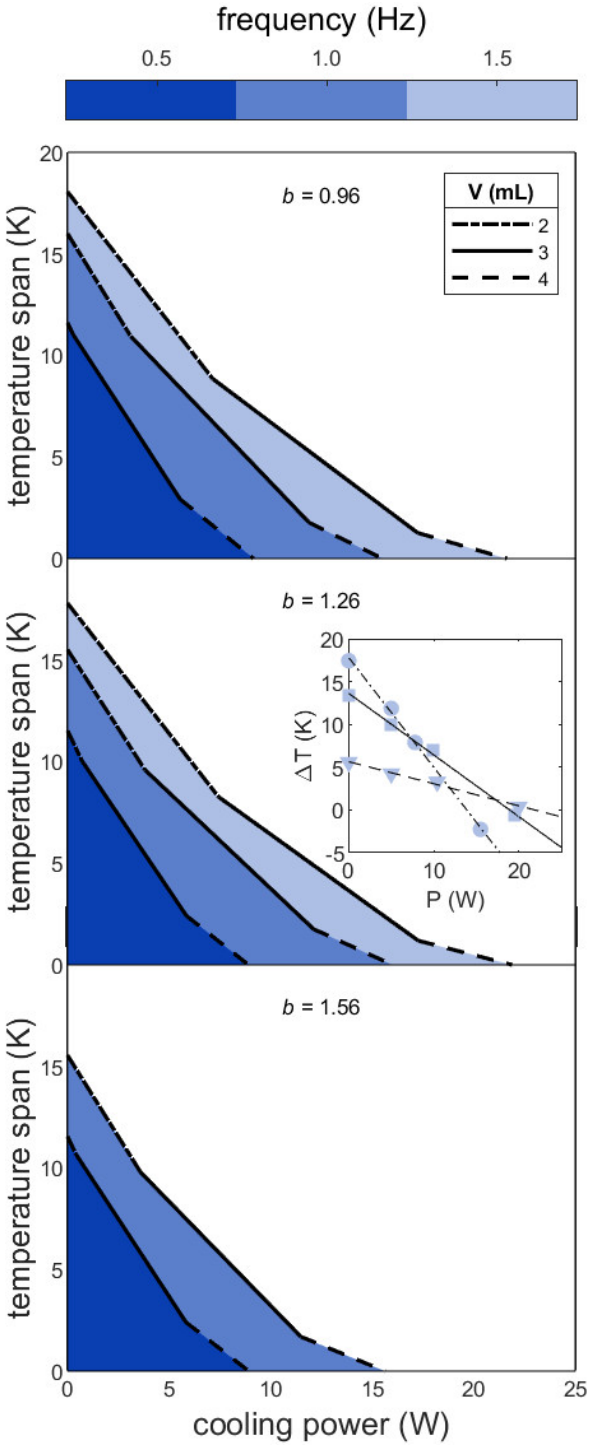

Figure 3 – Cooling power and temperature span for b = 0.96, 1.26, and 1.56 shows very similar performance despite the significant differences in the magnetic field profile (color version available online). Inset in the middle shows datasets with the corresponding linear fits for 2 (●), 3 (■), and 4 (▼) mL flow volumes at 1.5 Hz.

Heat transfer analysis is used to further understand the insensitivity of exergetic cooling power to the magnetic field profile. Using a frequency based solely on t_l (the lower of the two), the calculated heat transfer efficiency [14] remains greater than 0.99 for all three magnet profiles. This owes largely to the small, 200 µm particle size employed in CaloriSMART. The heat transfer efficiency for the typical particle diameters of 500 µm falls to 0.96 at a frequency of 1 Hz and 0.93 at 2 Hz. Even though the time for heat transfer decreases with decreasing t_l, the small spheres can still exchange essentially all of the heat generated from the magnetocaloric effect with the flowing fluid. As t_l shrinks, however, aligning the center of the magnetic field and fluid flow profiles results in sustained fluid flow when the magnetic field begins to change direction. The negative effect this has on regenerator performance is explained in Section 4.2.

Though experimentally we could not achieve the rotational acceleration necessary to demonstrate performance with $b < 0.96$, this case is explored with 1-D heat transfer modeling [15,20]. Magnetic field profiles with t_h and t_l the same as the profiles examined experimentally and those with the two values flipped, as shown in Figure S1, were simulated. Figure 5 shows the resulting exergetic cooling powers normalized by the $b = 0.96$ case both predicted by the model and measured. The modeling results and experimental results

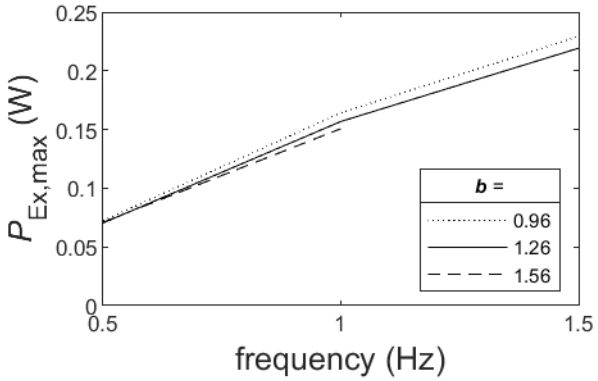

Figure 4 – Maximum exergetic cooling power as a function of frequency for $b = 0.96$, 1.26, and 1.56 in dotted, solid, and dashed lines, respectively.

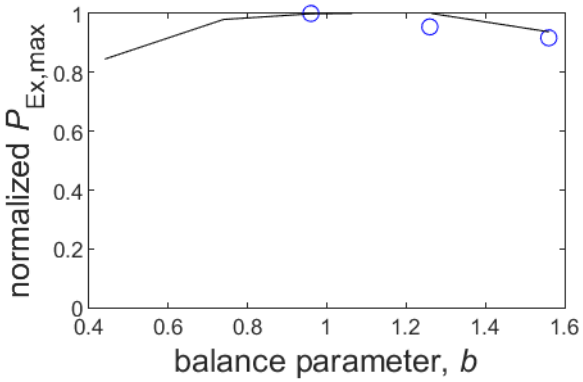

Figure 5 – Normalized exergetic cooling power as a function of the balance parameter measured (open points) and predicted by the heat transfer model (solid line).

qualitatively match very well, however, the model generally predicts less of a decrease in exergetic cooling power as b increases. For decreasing b, the model predicts a decrease in $P_{\mathrm{Ex,max}}$ of 2% for $b = 0.74$ and 16% for $b = 0.44$. Since the permanent magnet volume in the array scales roughly linearly with t_{h}, these results show that the permanent magnet volume (and cost) can be reduced by 20% with little impact on exergetic cooling power, or by 44% with about a 16% decrease in performance.

4.2 Fluid Flow Profile

Since the experimentally observed impact of the magnetic field profile is small, the constant rpm profile, b = 1.26, is used to explore the effects of ϕ and t_{d}. Figure 6 shows 360 measurements of temperature span as a function of t_{d} for a flow volume of 2 mL (utilization of 0.95 [9]), an operating frequency of 1 Hz, pump fractions from 0.3 to 0.8, and applied cooling loads from 0 to 7.5 W. Five values of t_{d} are examined for each pump fraction with the center value aligning the centers of the two profiles. For longer pump times, the flow must start sooner relative to the beginning of t_{l} to keep the centers of the two profiles aligned. Negative delay times mean the flow is started before the magnetic field has reached its minimum value. Vertical lines for the center points of each set show representative standard deviations for three independent runs with identical delay time and pump fraction.

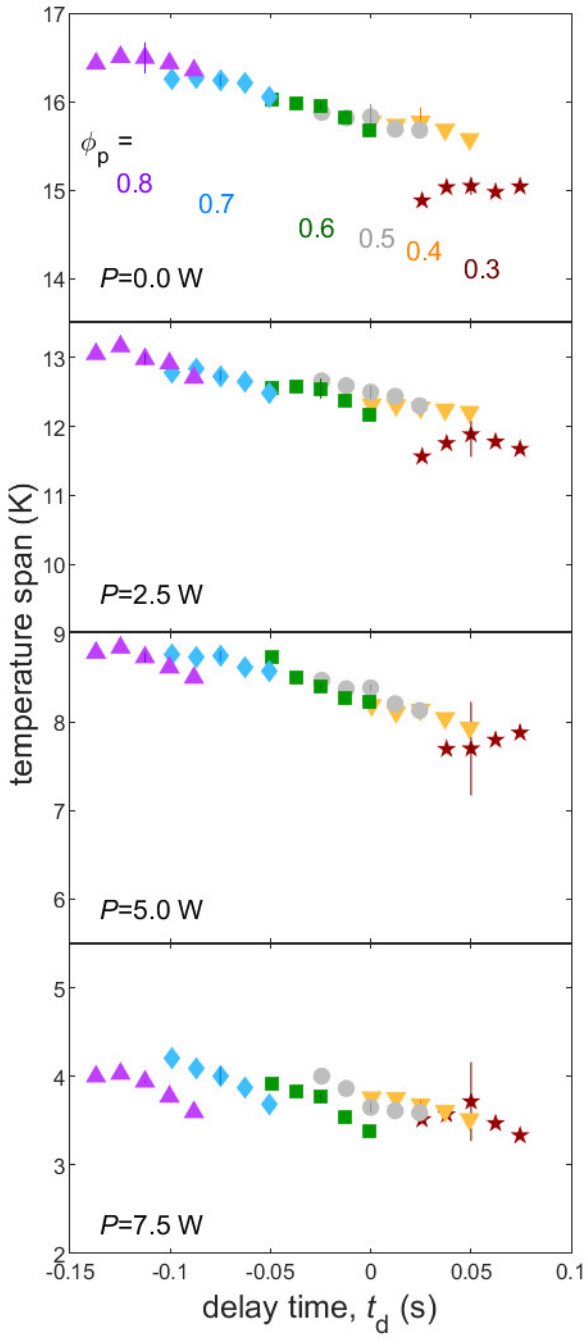

Figure 6 – Temperature span as a function of delay time, t_d, for cooling powers from 0 to 7.5 W and pump fractions of 0.8 (▲), 0.7 (◆), 0.6 (■), 0.5 (●), 0.4 (▼), and 0.3 (★). Vertical lines (in most cases smaller than the size of the symbol) for the center point of each set show representative standard deviation for three runs (color version available online).

The temperature span generally increases with increasing pump fraction except between 0.7 and 0.8 at 7.5 W cooling load. Though the impact of pump fraction on temperature span is small (note

that the temperature axis in Figure 6 is continuous across the four panels), larger pump fractions reduce the flow velocity. Pumping power, which scales with the square of flow velocity according to the Ergun equation [21], is a principal power expenditure [5]. Though it is known that increasing the pump fraction can increase device efficiency, Figure 6 additionally shows that the temperature span can be maintained or even improved at higher pump fractions for a fixed fluid flow volume (fixed regenerator utilization [22]).

Without applied cooling load, differences in the temperature span around the t_{d} that aligns the centers of the two profiles were within experimental variability. As the cooling power increases, however, the temperature span begins to decrease with increasing t_{d} for pump fractions of 0.4 and above until at the highest cooling power, the leftmost value of the t_{d} gives the maximum temperature span. This shows that as cooling power increases, the alignment between the flow rate profile and the magnetic field profile that yields the best performance shifts from center-aligned toward end-aligned. Qualitatively, aligning the centers of the two profiles ensures that there is sufficient temperature difference between the solid and the fluid when the fluid starts flowing, which is especially important at low pump fractions. Aligning the ends of the two profiles, on the other hand, ensures that the fluid does not flow after the magnetic field starts changing in the opposite direction, which is especially important at large pump fractions. Figure 7 shows the two extremes of center-aligned, and end-aligned profiles for a pump fraction of 0.8 along with the magnetic field profile. As can be seen from the relative sizes of the shaded areas in Figure 7, aligning the end of the flow with the end of the shorter of the two dwell times, t_{l} and t_{h}, will provide the maximum benefit.

5. Discussion

Importantly, changing t_{d} does not change the energy consumption of the system. Tuning it carefully eliminates the performance limitations at high pump fraction described elsewhere [10,11] which will further improve device efficiency at higher pump fractions. The device efficiency is expressed by the coefficient of performance,

$$COP = P/P_{\mathrm{d}} \tag{4}$$

where P_{d} is the power consumed by the device.

The thermodynamic limit of cycle efficiency for pumping heat from a lower temperature, T_{c}, to a higher temperature, T_{h}, is achieved by the Carnot cycle, making its efficiency COP_{Carnot},

$$COP_{\mathrm{Carnot}} = \frac{T_{\mathrm{c}}}{T_{\mathrm{h}} - T_{\mathrm{c}}} \tag{5}$$

useful for normalizing device efficiency. The so-called second-law (or exergy) efficiency, η, is also related to the exergetic cooling power described earlier

$$\eta = \frac{COP}{COP_{\mathrm{Carnot}}} = \frac{P_{\mathrm{Ex}}}{P_{\mathrm{d}}}. \tag{6}$$

Projecting the conservative efficiency improvements for maintaining the same temperature span at higher pump fractions for other systems provides a basis of comparison for the efficiency estimates for the CaloriSMART.

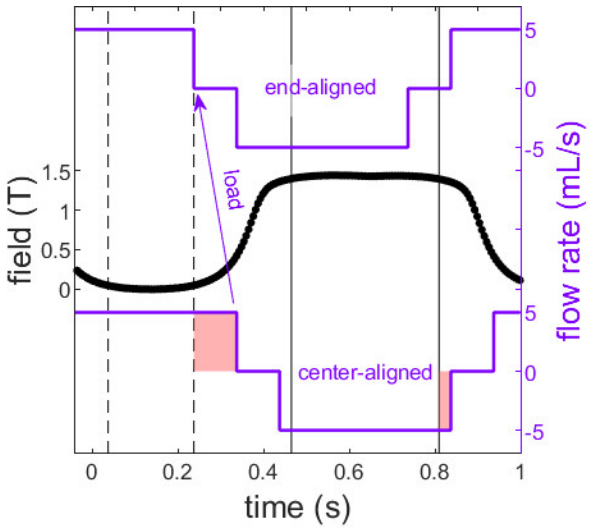

Figure 7 – For large pump fractions, the optimum t_d shifts from nearly a center-aligned case at no applied cooling load toward the end-aligned case at higher cooling loads to avoid flow after the magnetic field change reverses directions as in the area shaded in red (color version available online).

Fortkamp *et al.* report $\eta = 0.191$ [11] at a pump fraction of 0.8. Increasing the temperature span for pump fraction of 0.8 to be consistent with the reported COP_{Carnot} at pump fraction of 0.5 would increase this value to $\eta = 0.26$; about a 35% increase. Rather than normalizing by P_{d}, Teyber *et al.* define η^* which normalizes P_{Ex} by the power required to pump the heat exchange fluid, P_{p}, based on the measured pressure drop across the regenerator, ΔP, cycle time, t_{c}, and volumetric flow rate, $\dot{V}$, [10]

$$\eta^* = \frac{P_{\mathrm{Ex}}}{P_{\mathrm{p}}}, \qquad P_{\mathrm{p}} = \frac{1}{t_{\mathrm{c}}}\int_0^{t_{\mathrm{c}}} \dot{V}\Delta P dt. \qquad (7)$$

Under conditions where no flow is diverted, or $\phi_{\mathrm{p}} = 1$, they measure a maximum $\eta^* = 0.38$. Raising the exergetic cooling power to that achieved at their optimal pump fraction increases this value to 0.41, about a 7% increase. Based on a previously reported pumping power across the regenerators [5], we estimate $\eta^* = 0.61$ for results from Fortkamp *et al.* Figure S2 shows how the pumping power estimated using Equation (7) falls parabolically with ϕ_{p} for the CaloriSMART.

The highest η^* achieved in this study is 0.79 with a temperature span of 8.84 K at 5 W applied cooling power, $\phi_{\mathrm{p}} = 0.8$, and $t_{\mathrm{d}} = -0.125$ s. Though some of this improvement over the results of Teyber *et al.* may owe to the higher operating frequency of 1 Hz vs. 0.8 Hz, it clearly demonstrates the importance of balancing the magnetic field profile and matching the fluid flow profile. Since the magnet and pump motors of CaloriSMART are oversized for versatility [9], measuring the coefficient of performance of the system is unrealistic. Comparing the available results to other state of the art systems shows that the efficiency increase for adjusting the offset for higher ϕ_{p} could more than compensate for the 16% loss in performance we estimated with heat transfer modeling for reducing the active volume of the magnet assembly by 44%.

6. Conclusions

Making use of the unique capabilities provided by the fully digital and automated controls of the earlier reported CaloriSMART, we were able to achieve unprecedented control over the magnetic field and fluid flow profiles and the synchronization between the two. Our experiments indicate that effective heat exchange between properly sized active material particles and flowing water is possible even when the duration of the high magnetic field dwell time is cut in half. This insensitivity to the length of time that high magnetic field must be maintained could be leveraged to cut the volume and cost of permanent magnet assemblies in half by implementing designs with shorter high magnetic field periods or to double the amount of refrigerant activated by a given magnet volume, thus doubling the system cooling power. Varying both the t_{d} and pump fraction at several applied cooling loads, we show that the optimum t_{d} shifts from aligning the centers of the two profiles at low applied cooling loads toward aligning the ends of the two profiles at high cooling loads. Tailoring the t_{d} to the pump fraction maintains or improves temperature span with increasing pump fractions up to 0.8 at several applied cooling loads. Based on other reports, including both device efficiency and different pump fractions, this could increase the device efficiency anywhere from 8 to 35%. By increasing the ratio of the exergetic cooling power to the required pumping power compared to other devices by 30 to 100%, we show that device efficiency can be maintained or improved compared to the current state of the art while substantially reducing the costs associated with magnetic field sources.

Acknowledgements

This work was performed with joint funding from the Advanced Manufacturing Office and the Building Technologies Office of the Office of Energy Efficiency and Renewable Energy of the United States Department of Energy. Ames Laboratory is operated for the U.S. Department of Energy by

Iowa State University of Science and Technology under Contract No. DE-AC02-07CH11358.

Data availability statement

Experimental data are available upon reasonable request to the corresponding author.

Competing Interests

The Authors declare no competing interests

References

[1] Calm JM. The next generation of refrigerants - Historical review, considerations, and outlook. International Journal of Refrigeration 2008; 31:1123–33. https://doi.org/10.1016/j.ijrefrig.2008.01.013.

[2] Calm JM, Didion DA. Trade-offs in refrigerant selections: Past, present, and future. International Journal of Refrigeration 1998; 21:308–21. https://doi.org/10.1016/S0140-7007(97)00089-3.

[3] Global Cooling Prize. The Need n.d. https://globalcoolingprize.org/about-the-global-cooling-prize/the-need/ (accessed April 29, 2020).

[4] Goetzler W, Shandross R, Young J, Petritchenko O, Ringo D, McClive S. Energy Savings Potential and RD&D Opportunities for Commercial Building HVAC Systems. US Department of Energy 2017. https://doi.org/10.2172/1419622.

[5] Eriksen D, Engelbrecht K, Haffenden Bahl CR, Bjørk R, Bahl CRH, Bjørk R. Exploring the efficiency potential for an active magnetic regenerator. Science and Technology for the Built Environment 2016;22:527–33. https://doi.org/10.1080/23744731.2016.1173495.

[6] Russek SL, Zimm CB. Potential for cost effective magnetocaloric air conditioning systems. International Journal of Refrigeration 2006;29:1366–73. https://doi.org/10.1016/J.IJREFRIG.2006.07.019.

[7] Barclay JA, Steyert WA. Active magnetic regenerator. U.S. Patent No. 4,332,135, 1982.

[8] Giauque WF. A thermodynamic treatment of certain magnetic effects. A proposed method of producing temperatures considerably below 1 absolute. Journal of the American Chemical Society 1927;49:1864–70. https://doi.org/10.1021/ja01407a003.

[9] Griffith L, Czernuszewicz A, Slaughter J, Pecharsky V. CaloriSMART: Small-scale test-stand for rapid evaluation of active magnetic regenerator performance. Energy Conversion and Management 2019. https://doi.org/10.1016/j.enconman.2019.111948.

[10] Teyber R, Trevizoli P v., Niknia I, Christiaanse T v., Govindappa P, Rowe A. Experimental performance investigation of an active magnetic regenerator subject to different fluid flow waveforms. International Journal of Refrigeration 2017;74:38–46. https://doi.org/10.1016/j.ijrefrig.2016.10.001.

[11] Fortkamp FP, Eriksen D, Engelbrecht K, Bahl CRH, Lozano JA, Barbosa JR. Experimental investigation of different fluid flow profiles in a rotary multi-bed active magnetic regenerator device. International Journal of Refrigeration 2018;91:46–54. https://doi.org/https://doi.org/10.1016/j.ijrefrig.2018.04.019.

[12] Nakashima ATDD, Dutra SL, Trevizoli P v., Barbosa JR. Influence of the flow rate waveform and mass imbalance on the performance of active magnetic regenerators. Part I: Experimental analysis. International Journal of Refrigeration 2018;93:236–48. https://doi.org/10.1016/j.ijrefrig.2018.07.004.

[13] Aliev AM, Batdalov AB, Khanov LN, Koledov V v., Shavrov VG, Tereshina IS, et al. Magnetocaloric effect in some magnetic materials in alternating magnetic fields up to 22 hz. Journal of Alloys and Compounds 2016;676:601–5. https://doi.org/10.1016/j.jallcom.2016.03.238.

[14] Engelbrecht KL, Nellis GF, Klein SA. The Effect of Internal Temperature Gradients on Regenerator Matrix Performance. Journal of Heat Transfer 2006;128:1060–9. https://doi.org/10.1115/1.2345428.

[15] Engelbrecht K. A numerical model of an active magnetic regenerator refrigerator with experimental validation. ProQuest, 2008.

[16] Wakao N, Kaguei S, Funazkri T. Effect of fluid dispersion coefficients on particle-to-fluid heat transfer coefficients in packed beds: correlation of Nusselt numbers. Chemical Engineering Science 1979;34:325–36. https://doi.org/10.1016/0009-2509(79)85064-2.

[17] Bjørk R, Engelbrecht K. The influence of the magnetic field on the performance of an active magnetic regenerator (AMR). International Journal of Refrigeration 2011;34:192–203. https://doi.org/10.1016/j.ijrefrig.2010.07.004.

[18] Fortkamp F, Lang G, Lozano J, Barbosa J. Numerical analysis of the influence of magnetic field waveforms on the performance of active magnetic regenerators. Journal of the Brazilian Society of Mechanical Sciences and Engineering 2020;42:1–17.

[19] Benedict MA, Sherif SA, Beers DG, Schroeder MG. Design and performance of a novel magnetocaloric heat pump. Science and Technology for the Built Environment 2016;22:520–6.

[20] Lei T, Engelbrecht K, Nielsen KK, Veje CT. Study of geometries of active magnetic regenerators for room temperature magnetocaloric refrigeration. Applied Thermal Engineering 2015;111. https://doi.org/http://dx.doi.org/10.1016/j.applthermaleng.2015.11.113.

[21] Ergun S. Fluid flow through packed columns. Chem Eng Prog 1952;48:89–94.

[22] Johnson JE. Regenerator heat exchangers for gas turbines. Reports and Memoranda 1948.